Applied Physics Letters

The recombination mechanisms leading to amplified spontaneous emission at the true-green wavelength in $CH_3NH_3PbBr_3$ perovskites

Cite as: Appl. Phys. Lett. **106**, 081902 (2015); https://doi.org/10.1063/1.4913463
Submitted: 10 December 2014 • Accepted: 11 February 2015 • Published Online: 23 February 2015

D. Priante, I. Dursun, M. S. Alias, et al.

The recombination mechanisms leading to amplified spontaneous emission at the true-green wavelength in $CH_3NH_3PbBr_3$ perovskites

D. Priante,[1,a)] I. Dursun,[2,a)] M. S. Alias,[1] D. Shi,[2] V. A. Melnikov,[2] T. K. Ng,[1] O. F. Mohammed,[2] O. M. Bakr,[2] and B. S. Ooi[1,b)]

[1]*Photonics Laboratory, Computer, Electrical, and Mathematical Sciences and Engineering (CEMSE), King Abdullah University of Science & Technology (KAUST), Thuwal, 23955-6900, Saudi Arabia*

[2]*Solar & Photovoltaics Engineering Research Center (SPERC), Physical Sciences and Engineering (PSE), King Abdullah University of Science & Technology (KAUST), Thuwal, 23955-6900, Saudi Arabia*

(Received 10 December 2014; accepted 11 February 2015; published online 23 February 2015)

We investigated the mechanisms of radiative recombination in a $CH_3NH_3PbBr_3$ hybrid perovskite material using low-temperature, power-dependent (77 K), and temperature-dependent photoluminescence (PL) measurements. Two bound-excitonic radiative transitions related to grain size inhomogeneity were identified. Both transitions led to PL spectra broadening as a result of concurrent blue and red shifts of these excitonic peaks. The red-shifted bound-excitonic peak dominated at high PL excitation led to a true-green wavelength of 553 nm for $CH_3NH_3PbBr_3$ powders that are encapsulated in polydimethylsiloxane. Amplified spontaneous emission was eventually achieved for an excitation threshold energy of approximately 350 $\mu J/cm^2$. Our results provide a platform for potential extension towards a true-green light-emitting device for solid-state lighting and display applications. [http://dx.doi.org/10.1063/1.4913463]

Currently, green emitters with a wavelength less than 530 nm are dominated by InGaN-based inorganic materials. However, beyond 520 nm, toward a true-green wavelength of 555 nm, high lattice- and thermal-mismatch cause the nucleation of threading dislocations in materials with a drastic reduction in internal quantum efficiency, which constitutes the efficiency roll-over and "green gap" in solid-state lighting.[1] An investigation into alternative materials technology reveals that high photoluminescence quantum efficiency (PLQE) of approximately 70% has been demonstrated in solution-processed organic-inorganic hybrid perovskite semiconductors.[2] Previous studies have successfully identified materials for light emitters in the form of vertical microcavities,[2,3] whispering gallery cavities,[4] spherical resonators,[5] and free cavity.[6] Light-emitting diodes (LEDs) that radiate from visible to near-infrared light were achieved by tuning the halide compositions in $CH_3NH_3PbX_3$, where X = Br, I, and/or Cl.[7]

In the mixed halide perovskite material system, studies of optical and charge-carrier properties have focused on iodide, chloride, and mixed iodide-chloride halides. These studies explore temperature-dependent optical absorption[8] and photoluminescence (PL),[9] carrier recombination and mobility,[10] electron-hole transport,[11] recombination lifetimes,[12] dynamic bandgap shifts,[13] and carrier diffusion.[14,15] Further investigations on the carrier recombination dynamics leading to the efficient light emission are essential for eventual device application. In this paper, we study the recombination mechanisms of the bromide perovskites, which is relevant for realizing a true-green emitter.

The $CH_3NH_3PbBr_3$ powders were condensed out of solution by completely evaporating the solvent from a solution of equimolar $PbBr_2$ and CH_3NH_3Br in N,N-dimethylformamide. The device was then fabricated by curing the $CH_3NH_3PbBr_3$ powders that contain polydimethylsiloxane (PDMS) sandwiched between two sapphire substrates to obtain a flat layer ($CH_3NH_3PbBr_3$/PDMS henceforth). The powder X-ray diffraction (XRD) plot (Fig. 1) demonstrates the complete phase purity of the material and its correspondence with the room-temperature (RT) cubic-$CH_3NH_3PbBr_3$ perovskite structure.[16,17]

Using PL measurements, we show the radiative recombination mechanisms for $CH_3NH_3PbBr_3$ and demonstrated its ASE as follows. A continuous wave (CW) 473 nm laser was employed to measure PL, whereas the femtosecond laser pulsing at 475 nm was employed for the ASE measurements. These pulses were generated in an optical parametric amplifier, which was pumped with a 900 mW fundamental output of a Ti:sapphire regenerative amplifier that operates at 800 nm with 35 fs pulses and a repetition rate of 1 kHz.

Figure 2(a) shows the PL spectra at 77 K (−196 °C) and a CW laser incident power variation from 0.8–80 μW. We note that a broad hump and asymmetric narrow peak dominated the radiative recombination processes, which correspond to

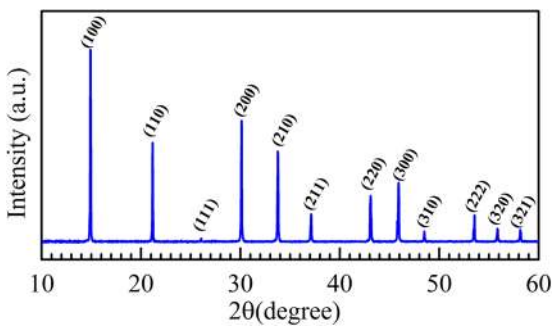

FIG. 1. XRD profile of $CH_3NH_3PbBr_3$ powders.

[a)]D. Priante and I. Dursun contributed equally to this work.
[b)]Email: boon.ooi@kaust.edu.sa

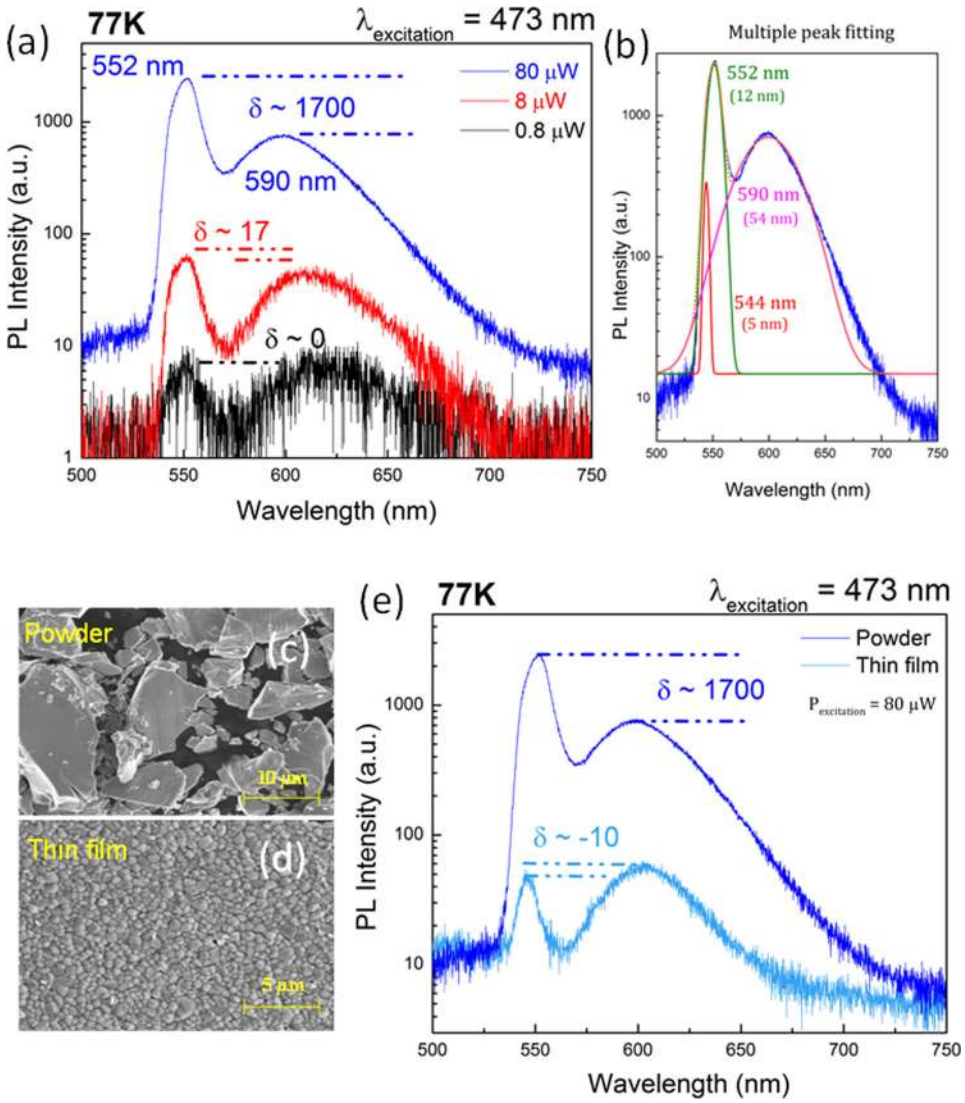

FIG. 2. (a) 77 K power dependent PL spectra of $CH_3NH_3PbBr_3$ powder; (b) multiple-Gaussian-peak fitting for the blue curve in (a) with peak wavelengths shown and FWHM values indicated in brackets; SEM images shows the morphology of: (c) powder (inhomogeneous grain sizes) and (d) thin film (comparatively homogeneous grain sizes) samples; (e) comparison of PL spectra for the $CH_3NH_3PbBr_3$ powder and thin film samples.

emissions from the bulk defect states, and the surface defect states, respectively, as explained in the following. The blue curve in Fig. 2(a) exhibits peak emission wavelengths of 552 nm (2.246 eV) and 590 nm (2.102 eV), respectively. When the PL spectrum at an excitation power of 80 μW was deconvoluted with three Gaussian peaks (see Fig. 2(b)), two of them showed FWHM of 5 nm and 12 nm, originated from the above narrow peak, while the third one corresponds to the broad hump with FWHM of 54 nm. Regarding the origin of the third Gaussian peak, we note that the peak intensities difference between the narrow peak and the broad hump, δ, was comparable at an excitation power of 0.8 μW. When the excitation power was increased from 8 μW to 80 μW, the δ value increased by one-hundred-fold. The result indicates a defect-like signature for the broad hump with a limited density of states. Therefore, the PL intensities saturated as photo-generated excess carriers began to fill the available states. For cases in which $CH_3NH_3PbBr_3$ single crystals are synthesized in our laboratory,[14] the above defect hump was not observed. This finding supports our attribution of the PL hump to bulk defects.

As for the deconvoluted peaks at 544 nm and 552 nm, they were attributed to inhomogeneity in the particles or the grain size of the powders sample. These results are expected due to the different surface states that populated over surfaces or cracks within the bulk of the as-synthesized powder (see Fig. 2(c)). For comparison, the thin film $CH_3NH_3PbBr_3$ sample was sequentially prepared using $PbBr_2$ spin coating and vapor-assisted deposition[18] of CH_3NH_3Br, which showed more uniform and homogeneous particles (see Fig. 2(d)). Consequently, the PL spectrum for this sample showed only one narrow peak and one broad hump related to surface states and bulk defects recombinations (see Fig. 2(e)). The δ value of -10 for the thin film sample as shown in Fig. 2(e) indicated a stronger bulk defects recombination in the thin film sample, which is due to the less crystallinity.

To ascertain the contribution of the bulk defect states as the photon absorption centers, we perform temperature dependent PL measurements. As shown in Fig. 3, the broad hump is pronounced at $-196\,^{\circ}$C but disappeared toward 16 $^{\circ}$C and RT, indicating an insignificant contribution of the bulk defect states at RT. This finding indicates an acceptable starting material for light emitters, which is consistent with the results from the powder XRD measurement in Fig. 1.

In addition, the surface state related peaks are asymmetric at both $-196\,^{\circ}$C and RT (refer to the bottom inset in Fig. 3), which is indicative of varying radiative recombination processes. The observed PL peak wavelength at $-196\,^{\circ}$C is

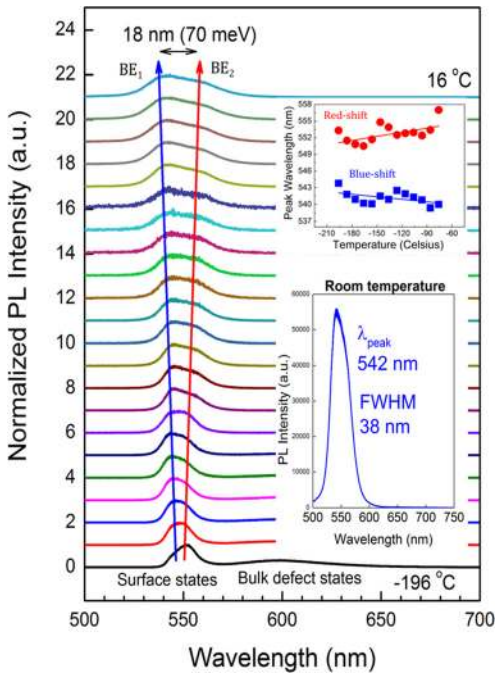

FIG. 3. Normalized temperature dependent PL spectra excited using a CW 473 nm laser excitation wavelength that shows both surface states and bulk defect states related recombinations. Insets show the temperature dependent wavelength shift for the deconvoluted surface states related radiative recombinations, which are denoted as BE_1 (blue-shift) and BE_2 (red-shift) at the top right, and the RT spectrum at the bottom right.

similar to the 549 nm excitonic peak observed at −268 °C by Tanaka *et al.*[19] We drew two trend lines to represent the blue- and red-shifting phenomena in Fig. 3. The deconvolution of the spectra was also performed, within the temperature range that was best fitted with Gaussian functions (refer to the top inset in Fig. 3), to better illustrate the phenomena. This is due to the simultaneous emission from two dominant surface states, denoted as bound excitons 1 and 2 (BE_1 and BE_2, respectively) in Fig. 3. This is consistent with the explanation of the grain size inhomogeneity in Fig. 2. It is noted that the range of BE values from 19–50 meV was previously reported for iodide perovskite materials;[13] therefore, our assumption of the BE surface states recombination is relevant. The blue-shift is most likely due to the *Burstein Moss* band filling effect,[12] which shows an increase in the bandgap. Although the band-filling effect dominated the temperature-dependent PL spectra at low temperatures, the red-shift of the BE_2 becomes pronounced with an increase in temperature. At 16 °C, the maximum peak separation was 18 nm (approximately 70 meV). The reason for the red-shift is clear when we consider the possible strong absorption in the BE_2 surface states, which originates from the existence of high density of surface-states in BE_2, and carrier filling in BE_2 due to excitation from the high energy photons from BE_1. Thus, BE_1 serves as the optical pump for the smaller and effective bandgap BE_2 surface states. This result may have caused a sustained ASE in the following.

Figure 4 shows the normalized PL intensity *versus* wavelength for the $CH_3NH_3PbBr_3$ powder/PDMS sample when optically pumped with 475 nm laser pulses. When optical excitation increases, approximately 553 nm BE_2 peak continues to dominate, and the normalized spectra exhibit a

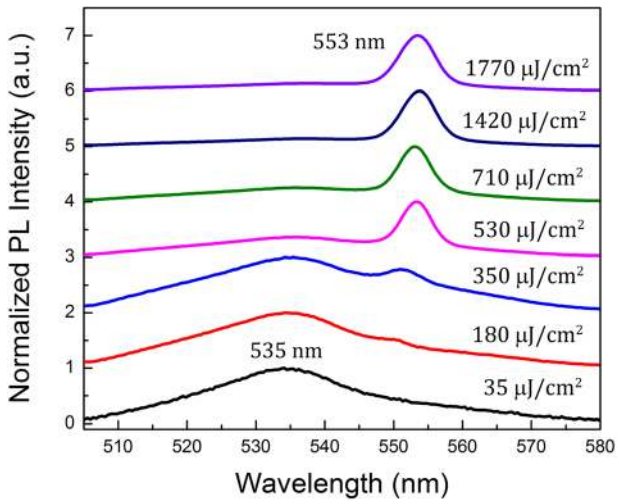

FIG. 4. Evolution of PL spectra with increasing optical pump fluence at 475 nm for the $CH_3NH_3PbBr_3$ powder/PDMS sample. The peak wavelength shifted from approximately 535 nm (BE_1) to approximately 553 nm (BE_2) with the increase in pump fluence.

significantly weaker 535 nm peak related to BE_1. The sustained BE_2 emission indicates increment in carriers accumulation and the probability of radiative recombination. When the PL intensity and FWHM as a function of pump fluence were extracted from the spectra in Figs. 5(a) and 5(b),

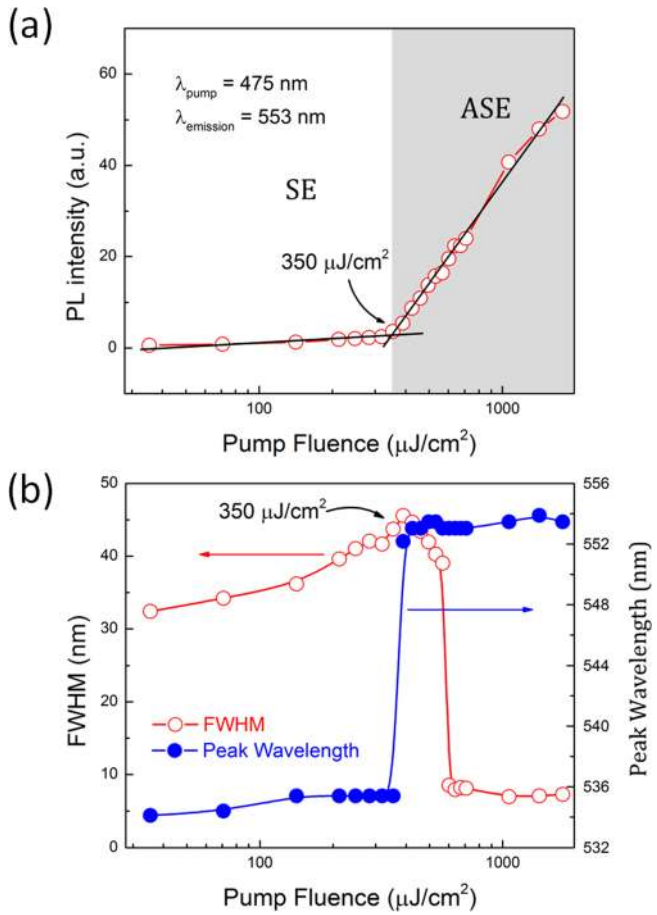

FIG. 5. Plot of (a) PL intensity *versus* pump fluence showing transition from spontaneous emission (SE) to amplified spontaneous emission (ASE). The fitted black lines are guides for the eyes; (b) FWHM and peak wavelength *versus* pump fluence for the same sample.

respectively, we obtained evidence of the PL transition from SE to ASE. The ASE peak wavelength occurred at 553 nm, which coincides with the BE_2 peak position, thus supporting the explanation on red-shift trend mentioned above, i.e., carrier excitation in BE_2 due to absorption of photons emitting from BE_1. The quantum yield was not measured here due to the unavailability of a suitable integrating sphere and related set-up. However, it is noted that the PLQE for the $CH_3NH_3PbBr_3$ film can be as high as 20%.[20,21]

The ASE threshold fluence is approximately 350 μJ/cm^2, where the intensity slope abruptly changes in conjunction with the reduction in FWHM from 44 to 40 nm and at sudden increase in wavelength from 535 nm to 553 nm as the pump fluence increases from 350 μJ/cm^2 to approximately 1770 μJ/cm^2.

We have identified the contribution of two different BE radiative transition signatures to the PL spectra of the $CH_3NH_3PbBr_3$ hybrid perovskite. For increasing temperatures, we observed concurrent blue- and red-shifting excitonic-peak wavelengths. Using high fluence optical pump energy for PL measurements, we explained the role of BE_2 in the ASE action in the bromide perovskite light emitter that operates at a 553 nm wavelength. These findings pave the way for further research on economical true-green lasers in the solid-state lighting and display applications.

The authors gratefully acknowledge the funding support from KAUST and King Abdulaziz City for Science and Technology TIC (Technology Innovation Center) for Solid-State Lighting at KAUST.

[1]F. C.-P. Massabuau, M. J. Davies, F. Oehler, S. K. Pamenter, E. J. Thrush, M. J. Kappers, A. Kovács, T. Williams, M. A. Hopkins, and C. J. Humphreys, Appl. Phys. Lett. **105**(11), 112110 (2014).
[2]F. Deschler, M. Price, S. Pathak, L. E. Klintberg, D.-D. Jarausch, R. Higler, S. Hüttner, T. Leijtens, S. D. Stranks, and H. J. Snaith, J. Phys. Chem. Lett. **5**(8), 1421 (2014).
[3]Z. Han, H.-S. Nguyen, F. Boitier, Y. Wei, K. Abdel-Baki, J.-S. Lauret, J. Bloch, S. Bouchoule, and E. Deleporte, Opt. Lett. **37**(24), 5061 (2012).
[4]Q. Zhang, S. T. Ha, X. Liu, T. C. Sum, and Q. Xiong, Nano Lett. **14**(10), 5995–6001 (2014).
[5]B. R. Sutherland, S. Hoogland, M. M. Adachi, C. T. O. Wong, and E. H. Sargent, ACS Nano **8**(10), 10947–10952 (2014).
[6]G. Xing, N. Mathews, S. S. Lim, N. Yantara, X. Liu, D. Sabba, M. Grätzel, S. Mhaisalkar, and T. C. Sum, Nat. Mater. **13**(5), 476 (2014).
[7]Z.-K. Tan, R. S. Moghaddam, M. L. Lai, P. Docampo, R. Higler, F. Deschler, M. Price, A. Sadhanala, L. M. Pazos, D. Credgington, F. Hanusch, T. Bein, H. J. Snaith, and R. H. Friend, Nat. Nanotechnol. **9**(9), 687 (2014).
[8]C. Wehrenfennig, M. Liu, H. J. Snaith, M. B. Johnston, and L. M. Herz, APL Mater. **2**(8), 081513 (2014).
[9]K. Wu, A. Bera, C. Ma, Y. Du, Y. Yang, L. Li, and T. Wu, Phys. Chem. Chem. Phys. **16**(41), 22476 (2014).
[10]C. Wehrenfennig, G. E. Eperon, M. B. Johnston, H. J. Snaith, and L. M. Herz, Adv. Mater. **26**(10), 1584 (2014).
[11]G. Xing, N. Mathews, S. Sun, S. S. Lim, Y. M. Lam, M. Grätzel, S. Mhaisalkar, and T. C. Sum, Science **342**(6156), 344 (2013).
[12]S. D. Stranks, G. E. Eperon, G. Grancini, C. Menelaou, M. J. P. Alcocer, T. Leijtens, L. M. Herz, A. Petrozza, and H. J. Snaith, Science **342**(6156), 341 (2013).
[13]J. S. Manser and P. V. Kamat, Nat. Photonics **8**(9), 737 (2014).
[14]D. Shi, V. Adinolfi, R. Comin, M. Yuan, E. Alarousu, A. Buin, Y. Chen, S. Hoogland, A. Rothenberger, K. Katsiev, Y. Losovyj, X. Zhang, P. A. Dowben, O. F. Mohammed, E. H. Sargent, and O. M. Bakr, Science **347**(6221), 519 (2015).
[15]Q. Dong, Y. Fang, Y. Shao, P. Mulligan, J. Qiu, L. Cao, and J. Huang, "Electron-hole diffusion lengths >175 μm in solution grown $CH_3NH_3PbI_3$ single crystals," Science (published online).
[16]A. Kojima, K. Teshima, Y. Shirai, and T. Miyasaka, J. Am. Chem. Soc. **131**(17), 6050 (2009).
[17]J. H. Noh, S. H. Im, J. H. Heo, T. N. Mandal, and S. I. Seok, Nano Lett. **13**(4), 1764 (2013).
[18]Q. Chen, H. Zhou, Z. Hong, S. Luo, H. S. Duan, H. H. Wang, Y. Liu, G. Li, and Y. Yang, J. Am. Chem. Soc. **136**(2), 622 (2014).
[19]K. Tanaka, T. Takahashi, T. Ban, T. Kondo, K. Uchida, and N. Miura, Solid State Commun. **127**(9), 619 (2003).
[20]S. Gonzalez-Carrero, R. E. Galian, and J. Pérez-Prieto, "Maximizing the emissive properties of $CH_3NH_3PbBr_3$ perovskite nanoparticles," J. Mater. Chem. A (published online).
[21]L. C. Schmidt, A. Pertegás, S. González-Carrero, O. Malinkiewicz, S. Agouram, G. M. Espallargas, H. J. Bolink, R. E. Galian, and J. Peŕez-Prieto, "Nontemplate synthesis of $CH_3NH_3PbBr_3$ perovskite nanoparticles," J. Am. Chem. Soc. **136**(3), 850–853 (2014).